Available online at www.sciencedirect.com
SCIENCE DIRECT®
Journal of Computational Physics 200 (2004) 238–250
JOURNAL OF COMPUTATIONAL PHYSICS
www.elsevier.com/locate/jcp

Perfectly matched layer for the time domain finite element method

Thomas Rylander *, Jian-Ming Jin

Center for Computational Electromagnetics, Department of Electrical and Computer Engineering, University of Illinois at Urbana-Champaign, 1406 West Green Street, Urbana, IL 61801-2991, USA

Received 26 July 2003; received in revised form 29 February 2004; accepted 8 March 2004
Available online 28 May 2004

Abstract

A new perfectly matched layer (PML) formulation for the time domain finite element method is described and tested for Maxwell's equations. In particular, we focus on the time integration scheme which is based on Galerkin's method with a temporally piecewise linear expansion of the electric field. The time stepping scheme is constructed by forming a linear combination of exact and trapezoidal integration applied to the temporal weak form, which reduces to the well-known Newmark scheme in the case without PML. Extensive numerical tests on scattering from infinitely long metal cylinders in two dimensions show good accuracy and no signs of instabilities. For a circular cylinder, the proposed scheme indicates the expected second order convergence toward the analytic solution and gives less than 2% root-mean-square error in the bistatic radar cross section (RCS) for resolutions with more than 10 points per wavelength. An ogival cylinder, which has sharp corners supporting field singularities, shows similar accuracy in the monostatic RCS.

PACS: 03.50.De; 41.20.Jb

Keywords: Perfectly matched layer; Time domain finite element method; Time integration; Dispersive material

1. Introduction

The perfectly matched layer (PML) is very popular and efficient for grid truncation of open-region problems. The PML concept was first introduced by Bérenger [1] in the context of solving Maxwell's equations. The original formulation by Bérenger was implemented in terms of the finite-difference time-domain (FDTD) [2] scheme and it involved a splitting of the electric and magnetic field components expressed in the Cartesian coordinate system. Chew and Weedon [3] interpreted the PML as a complex coordinate stretching, which is based on analytic continuation of Maxwell's equations to complex space.

* Corresponding author. Tel.: +1-217-333-1202; fax: +1-217-333-5962.
E-mail addresses: tryl@uiuc.edu (T. Rylander), j-jin1@uiuc.edu (J.-M. Jin).

0021-9991/$ - see front matter
doi:10.1016/j.jcp.2004.03.016

Shortly thereafter, Sacks et al. [4] used tensorial permittivity and permeability in Maxwell's equations to construct a PML. These three PML formulations are closely related [5–7] to each other. The split field formulation and anisotropic material formulation have been used extensively for time domain computations, mainly implemented in the context of the FDTD scheme. A compilation of articles on the PML associated with the FDTD scheme can be found in the book [8] by Taflove. In addition to formulations which are based on Cartesian coordinates, the PML can be formulated in cylindrical and spherical coordinate systems [9–11]. Apart from situations involving electromagnetic wave phenomena, the PML has been used successfully to truncate grids for wave problems in e.g. acoustics and mechanics.

The finite element method (FEM) [12] can handle unstructured grids that allow for accurate modeling of complex boundaries and local mesh refinement, which is challenging to treat within the framework of the FDTD scheme. The anisotropic material formulation of the PML suits the FEM well and it has mainly been used for computations in the frequency domain [13–16]. Tsai et al. [17] presented a time domain FEM scheme based on a modified anisotropic material, where the frequency dependence of the PML is approximated in an intuitive way. Their work is closely related to a non-dispersive formulation presented by Mathis [18]. However, the dispersive characteristics of the PML are important for a high level of absorption within a broad frequency band. Jiao et al. [19,20] worked on formulations for the time domain FEM which capture the frequency dependence of the PML accurately, where the dispersive characteristics are expressed in terms of recursive convolutions [25,8] involving the sought field. The two-dimensional algorithm [19] is based on the split field equations of Bérenger, where the spatial dependence of the PML conductivity is neglected. This scheme and the three-dimensional algorithm [20] evaluate the convolutions by exact integration under the assumption that the field is piecewise constant with respect to time, or trapezoidal integration if the field is assumed to be piecewise linear in time. The time integration procedure [20] mixes the Newmark scheme [26] and backward Euler. These are employed for the integration of the system of ordinary differential equations and auxiliary variables, respectively. Jiao et al. [19,20] also provide a stability analysis of their PML formulations for the time domain FEM. For the PML combined with the FDTD scheme based on exponential time differencing and standard time-averaging, Petropoulos [21] evaluated stability and accuracy in terms of the relaxation time scales associated with the electric and magnetic conduction currents that are present in the PML. Issues concerning the stability of the PML for the continuous Maxwell's equations are discussed in terms of symmetry by Turkel and Yefet [22], anisotropy by Bécache et al. [23] and causality by Teixeira and Chew [24].

In this article, we develop and test a new formulation for the FEM augmented with the PML in the context of the time dependent Maxwell's equations. The new scheme is inspired by the work by Jiao et al. [20], which can be derived from Maxwell's equations in the frequency domain with a PML represented by dispersive anisotropic materials [4]. Galerkin's method is used for the spatial discretization where the electric field is expanded in terms of edge elements [27]. The problem is then moved to the time domain and we use FEM concepts for the temporal discretization by introducing a piecewise linear temporal dependence for the electric field and employing Galerkin's method to construct the time integration scheme. The weak formulation with respect to time is evaluated by both exact and trapezoidal integration and we form a linear combination of the two, which is known as tunable integration [28]. This time stepping scheme specializes to the well-known Newmark scheme [26] in the case without PML and it treats the convolutions appearing in the PML region consistently. All convolutions are evaluated recursively by exact integration given that the field is a piecewise linear function in time. We emphasize that the proposed algorithm uses its time integration scheme in a consistent manner throughout the entire computational domain for all quantities in the continuous problem. Extensive numerical tests demonstrate that the new time stepping scheme can handle a very large number of time steps in a stable way. Galerkin's method in conjunction with a piecewise linear time dependence for the unknown field has been used successfully by Abboud et al. [29] for a stable solution of the retarded potential integral equations. We test our new formulation on radar cross section (RCS) computations in two dimensions. The RCS computations deal with infinitely long

metal cylinders of circular and ogival cross sections. It should be emphasized that the PML is directly applicable to both the scattered and the total field formulation of scattering problems as well as to radiating structures.

2. Formulation

The new time domain FEM formulation is demonstrated for the PML expressed in Cartesian and polar coordinates and, here, we focus on two-dimensional problems. Given a scatterer or radiating structure, the outward propagating wave is absorbed by a PML of finite thickness. We discretize the PML region by quadrilaterals and the PML is backed by a homogeneous Dirichlet boundary condition. The remaining part of the computational domain is discretized by triangles and/or quadrilaterals. A typical discretization is shown in Fig. 1 for a scatterer with the shape of a circular cylinder, where the computational domain is truncated by a PML tailored for polar coordinates.

2.1. Frequency domain

The derivation of our formulation is based on the PML interpreted as an anisotropic material [4]. For Maxwell's equations $\nabla \times \vec{\vec{\mu}}^{-1} \nabla \times \vec{E} + s^2 \vec{\vec{\epsilon}} \vec{E} = \vec{0}$ with the Laplace transform variable $s = \alpha + \mathrm{i}\omega$, we expand the electric field in terms of linear edge elements $\vec{N}_j$ and use Galerkin's method to derive the weak form

$$\int_S \left(\nabla \times \vec{N}_i \right) \cdot \vec{\vec{\mu}}^{-1} \cdot \left(\nabla \times \vec{E} \right) + s^2 \vec{N}_i \cdot \vec{\vec{\epsilon}} \cdot \vec{E} \, \mathrm{d}S = 0, \tag{1}$$

where we assume that the scatterer is a perfect electric conductor (PEC) and that the PML enclosing the scatterer is terminated by a homogeneous Dirichlet boundary condition. The weak form can be adapted to account for a variety of boundary conditions and sources. The anisotropic material parameters in Eq. (1) are given by $\vec{\vec{\mu}} = \mu_0 \vec{\vec{\Lambda}}$ and $\vec{\vec{\epsilon}} = \epsilon_0 \vec{\vec{\Lambda}}$, where

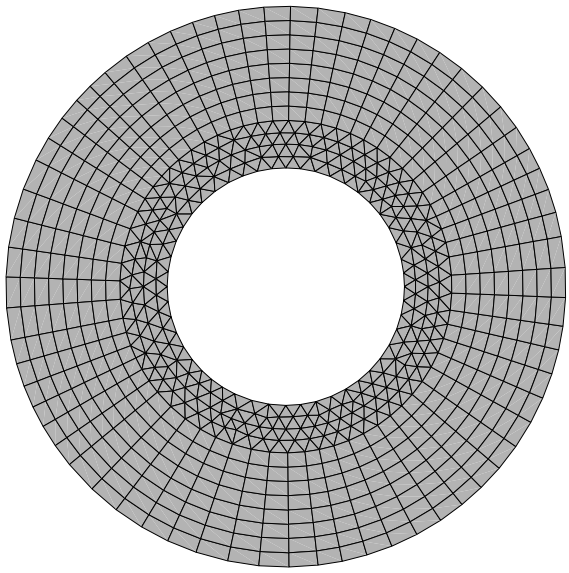

Fig. 1. Discretization for circular cylinder with a PML in polar coordinates.

$$\vec{\vec{\Lambda}} = \hat{u}\frac{\gamma_v}{\gamma_u}\hat{u} + \hat{v}\frac{\gamma_u}{\gamma_v}\hat{v} + \hat{z}\gamma_u\gamma_v\hat{z}, \tag{2}$$

$\gamma_u = 1 + s^{-1}\beta_u$ and $\gamma_v = 1 + s^{-1}\beta_v$. This expression can be used for the PML formulated in both Cartesian and polar coordinates [11]. In Cartesian coordinates, we substitute x for u and y for v which gives $\beta_x(x) = \epsilon_0^{-1}\sigma_x(x)$ and $\beta_y(y) = \epsilon_0^{-1}\sigma_y(y)$. Similarly, we replace u by r and v by ϕ for the PML in polar coordinates, where $\beta_r(r) = \epsilon_0^{-1}\sigma(r)$ and $\beta_\phi(r) = (\epsilon_0 r)^{-1}\int_0^r \sigma(r')\,\mathrm{d}r'$. In the physical region, which is void of the PML, we have $\gamma_u = \gamma_v = 1$ and $\vec{\vec{\Lambda}}$ reduces to the unity tensor.

2.2. Time domain

The time domain counterpart to Eq. (1) is obtained by the inverse Laplace transform, which gives a system of coupled ordinary differential equations (ODEs) with $\vec{E}(\vec{r},t) = \vec{0}$ for $t \leqslant 0$. The ith ODE is expressed as

$$\sum_j \left[S_{ij} + S_{ij}^{zz} + M_{ij} + B_{ij} + B_{ij}^{uu} + B_{ij}^{vv}\right] = 0, \tag{3}$$

where the indices i and j refer to spatial degrees of freedom associated with the edge elements. The terms in Eq. (3) are given by

$$S_{ij} = \left(\int_S \nabla\times\vec{N}_i\cdot\nabla\times\vec{N}_j\,\mathrm{d}S\right)E_j, \tag{4}$$

$$S_{ij}^{zz} = \int_S \nabla\times\vec{N}_i\cdot\hat{z}\left[\varphi_{zz}^{-1} * E_j\right]\hat{z}\cdot\nabla\times\vec{N}_j\,\mathrm{d}S, \tag{5}$$

$$M_{ij} = \left(\int_S \vec{N}_i\cdot\vec{N}_j\,\mathrm{d}S\right)\frac{\partial_t^2}{c^2}E_j, \tag{6}$$

$$B_{ij} = \left(\int_S \vec{N}_i\cdot\left[\hat{u}\frac{\beta_v-\beta_u}{c}\hat{u} + \hat{v}\frac{\beta_u-\beta_v}{c}\hat{v}\right]\cdot\vec{N}_j\,\mathrm{d}S\right)\frac{\partial_t}{c}E_j, \tag{7}$$

$$B_{ij}^{uu} = \int_S \vec{N}_i\cdot\hat{u}\left[\varphi_{uu} * \left(\frac{\partial_t}{c}E_j\right)\right]\hat{u}\cdot\vec{N}_j\,\mathrm{d}S, \tag{8}$$

$$B_{ij}^{vv} = \int_S \vec{N}_i\cdot\hat{v}\left[\varphi_{vv} * \left(\frac{\partial_t}{c}E_j\right)\right]\hat{v}\cdot\vec{N}_j\,\mathrm{d}S, \tag{9}$$

where c is the speed of light, the convolution operator is denoted by an asterisk

$$\varphi_{uu}(\vec{r},t) = -\frac{\beta_v-\beta_u}{c}\beta_u \mathrm{e}^{-\beta_u t}H(t), \tag{10}$$

$$\varphi_{vv}(\vec{r},t) = -\frac{\beta_u-\beta_v}{c}\beta_v \mathrm{e}^{-\beta_v t}H(t), \tag{11}$$

$$\varphi_{zz}^{-1}(\vec{r},t) = \left(\frac{\beta_u^2}{\beta_v-\beta_u}\mathrm{e}^{-\beta_u t} + \frac{\beta_v^2}{\beta_u-\beta_v}\mathrm{e}^{-\beta_v t}\right)H(t) \tag{12}$$

and Heaviside's step function is denoted by $H(t)$. Thus, the electric field is expressed as $\vec{E}(\vec{r},t) = \sum E_j(t)\vec{N}_j(\vec{r})$ where the time dependence of the coefficients $E_j(t)$ remains to be discretized. Note that the operators in Eqs. (4), (6) and (7) are factorized into a spatial and a temporal part. However, this is not possible for the operators in Eqs. (5), (8) and (9) due to the convolutions of functions with both spatial and temporal dependence.

2.3. Temporal discretization

We use a uniform discretization with respect to time and the time step is denoted Δt. Express the coefficient $E_j(t)$ as a piecewise linear function, i.e. $E_j(t) = \sum_m E_j^m T^m(t)$, where E_j^m is the unknown which corresponds to $E_j(t)$ evaluated at $t = m\Delta t$ for $m = 1, 2, \ldots$ Here, $T^m(t)$ is a piecewise linear basis function which satisfies $T^m(n\Delta t) = 0$ for $n \neq m$ and $T^m(m\Delta t) = 1$.

Convolutions of the type $\psi_j(\vec{r}, t) = \varphi(\vec{r}, t) * \mathscr{A}[E_j](t)$, which are found in Eq. (3), can be evaluated recursively for $\varphi(\vec{r}, t) = a\mathrm{e}^{-bt}$, where a and b are functions of $\vec{r}$. Here, $\mathscr{A}$ is the identity operator 1 or the time derivative ∂_t and, in the following, $\psi_j(\vec{r}, t)$ is used to denote either $\xi_j(\vec{r}, t) = \varphi(\vec{r}, t) * E_j(t)$ or $\zeta_j(\vec{r}, t) = \varphi(\vec{r}, t) * \partial_t E_j(t)$ in contexts where the same procedure or formula can be applied to both of them. We base the computation of the convolutions on the recursive relation

$$\psi_j(\vec{r}, t) = \mathrm{e}^{-b(t-t_1)}\psi_j(\vec{r}, t_1) + a\mathrm{e}^{-bt}\int_{t_1}^{t} \mathrm{e}^{b\tau}\mathscr{A}[E_j](\tau)\,\mathrm{d}\tau, \tag{13}$$

which is evaluated using exact integration given that $E_j(t) = \sum_m E_j^m T^m(t)$. In order to derive a recursive formula tailored for the computation of $\xi_j^{n-1}(\vec{r}) = \xi_j(\vec{r}, t^{n-1})$, we set $t = t^{n-1}$ and $t_1 = t^{n-2}$ in Eq. (13) which gives

$$\xi_j^{n-1}(\vec{r}) = \frac{a}{b^2\Delta t}\left(b\Delta t - 1 + \mathrm{e}^{-b\Delta t}\right)E_j^{n-1} + \frac{a}{b^2\Delta t}\left(1 - (1 + b\Delta t)\mathrm{e}^{-b\Delta t}\right)E_j^{n-2} + \mathrm{e}^{-b\Delta t}\xi_j^{n-2}(\vec{r}). \tag{14}$$

Analogously, we recursively update convolutions which involve the time derivative of the electric field by

$$\zeta_j^{n-1}(\vec{r}) = \frac{a}{b\Delta t}\left(1 - \mathrm{e}^{-b\Delta t}\right)E_j^{n-1} - \frac{a}{b\Delta t}\left(1 - \mathrm{e}^{-b\Delta t}\right)E_j^{n-2} + \mathrm{e}^{-b\Delta t}\zeta_j^{n-2}(\vec{r}), \tag{15}$$

where $\zeta_j^{n-1}(\vec{r}) = \zeta_j(\vec{r}, t^{n-1})$.

Next, we focus on the derivation of a time stepping scheme for Eq. (3). The time stepping scheme is based on Galerkin's method where the temporal dependence of the electric field is piecewise linear, i.e. multiply Eq. (3) with $T^n(t)$ and integrate with respect to time. This integration can be performed with either exact or trapezoidal integration, and we form a linear combination of the two with the weights 6θ and $1 - 6\theta$, respectively. Such a linear combination of different integration schemes is known as tunable integration [28]. Following this procedure, $E_j(t)$ in Eq. (4) is replaced by

$$\frac{1}{\Delta t}\int_0^\infty T^n(t)E_j(t)\,\mathrm{d}t = \theta E_j^{n+1} + (1 - 2\theta)E_j^n + \theta E_j^{n-1}$$

and, analogously, $\partial_t E_j(t)$ in Eq. (7) is given by $(E_j^{n+1} - E_j^{n-1})/(2\Delta t)$ while $\partial_t^2 E_j(t)$ in Eq. (6) is represented by $(E_j^{n+1} - 2E_j^n + E_j^{n-1})/(\Delta t)^2$. This time discretization is known as the Newmark scheme [26] and the parameter θ controls the degree of implicitness, where $\theta \geqslant 1/4$ guarantees unconditional stability [30]. For consistency, we use the same procedure to interpret the convolutions in Eqs. (5), (8) and (9). Consequently, we test a quantity $\psi_j(\vec{r}, t)$ with $T^n(t)$ to obtain

$$\begin{aligned}\frac{1}{\Delta t}\int_0^\infty T^n(t)\psi_j(\vec{r}, t)\,\mathrm{d}t = {} & \frac{1}{\Delta t}\left\{\int_0^\infty T^n(t)\mathrm{e}^{-b(t-t_1)}\,\mathrm{d}t\right\}\psi_j(\vec{r}, t_1) \\ & + \sum_m E_j^m\left\{\frac{1}{\Delta t}\int_0^\infty T^n(t)\left\{a\mathrm{e}^{-bt}\int_{t_1}^{t}\mathrm{e}^{b\tau}\mathscr{A}[T^m](\tau)\,\mathrm{d}\tau\right\}\mathrm{d}t\right\},\end{aligned} \tag{16}$$

where we use exact integration with respect to τ as previously for Eq. (13). We set $t_1 = (n-1)\Delta t$ and use either exact or trapezoidal integration with respect to t in Eq. (16). Exact integration gives

$$\frac{1}{\Delta t}\int_0^\infty T^n(t)\xi_j(\vec{r},t)\,\mathrm{d}t = \frac{a}{b}\left(\frac{1}{6}-\frac{1}{2b\Delta t}+\frac{1}{(b\Delta t)^2}-\frac{1-\mathrm{e}^{-b\Delta t}}{(b\Delta t)^3}\right)E_j^{n+1} + \frac{a}{b}\left(\frac{2}{3}-\frac{2}{(b\Delta t)^2}+\frac{3-(4-\mathrm{e}^{-b\Delta t})\mathrm{e}^{-b\Delta t}}{(b\Delta t)^3}\right)E_j^{n} + \frac{a}{b}\left(\frac{1}{6}+\frac{1}{2b\Delta t}+\frac{\mathrm{e}^{-b\Delta t}(2-\mathrm{e}^{-b\Delta t})}{(b\Delta t)^2}+\frac{(3-\mathrm{e}^{-b\Delta t})\mathrm{e}^{-b\Delta t}-2}{(b\Delta t)^3}\right)E_j^{n-1} + \left(\frac{1-\mathrm{e}^{-b\Delta t}}{b\Delta t}\right)^2\xi_j^{n-1}(\vec{r}) \tag{17}$$

and

$$\frac{1}{\Delta t}\int_0^\infty T^n(t)\zeta_j(\vec{r},t)\,\mathrm{d}t = \frac{a}{b\Delta t}\left(\frac{1}{2}-\frac{1}{b\Delta t}+\frac{1-\mathrm{e}^{-b\Delta t}}{(b\Delta t)^2}\right)E_j^{n+1} + \frac{a}{(b\Delta t)^2}\left(2+\frac{(4-\mathrm{e}^{-b\Delta t})\mathrm{e}^{-b\Delta t}-3}{b\Delta t}\right)E_j^{n} + \frac{a}{b\Delta t}\left(-\frac{1}{2}-\frac{1}{b\Delta t}+\frac{2-(3-\mathrm{e}^{-b\Delta t})\mathrm{e}^{-b\Delta t}}{(b\Delta t)^2}\right)E_j^{n-1} + \left(\frac{1-\mathrm{e}^{-b\Delta t}}{b\Delta t}\right)^2\zeta_j^{n-1}(\vec{r}) \tag{18}$$

while trapezoidal integration results in

$$\frac{1}{\Delta t}\int_0^\infty T^n(t)\xi_j(\vec{r},t)\,\mathrm{d}t = a\Delta t\left(\frac{b\Delta t-(1-\mathrm{e}^{-b\Delta t})}{(b\Delta t)^2}\right)E_j^{n} + a\Delta t\left(\frac{1-(1+b\Delta t)\mathrm{e}^{-b\Delta t}}{(b\Delta t)^2}\right)E_j^{n-1} + \mathrm{e}^{-b\Delta t}\xi_j^{n-1}(\vec{r}) \tag{19}$$

and

$$\frac{1}{\Delta t}\int_0^\infty T^n(t)\zeta_j(\vec{r},t)\,\mathrm{d}t = a\left(\frac{1-\mathrm{e}^{-b\Delta t}}{b\Delta t}\right)E_j^{n} - a\left(\frac{1-\mathrm{e}^{-b\Delta t}}{b\Delta t}\right)E_j^{n-1} + \mathrm{e}^{-b\Delta t}\zeta_j^{n-1}(\vec{r}). \tag{20}$$

Following the above recipe for the derivation of the Newmark scheme, we represent the convolution in Eq. (5) by forming a linear combination of Eqs. (17) and (19) weighted by 6θ and $1-6\theta$, respectively. Similarly, the convolutions in Eqs. (8) and (9) are represented by the linear combination of Eq. (18) weighted by 6θ and Eq. (20) weighted by $1-6\theta$. In this setting, ξ_j^{n-1} and ζ_j^{n-1} are updated recursively by Eqs. (14) and (15), respectively.

A naive evaluation of the coefficients in the convolution stencils gives catastrophic cancellation when $b\Delta t \to 0$. Consequently, accuracy is lost within the time stepping algorithm, which can cause instabilities. We expand such sensitive coefficients in Taylor series with 20 terms, which give roughly 16 accurate digits for $b\Delta t < 1$. The cancellation error in the original expressions for the coefficients is negligible for $b\Delta t \geqslant 1$ and the formulas given above yield highly accurate results.

In order to arrive at a practical time integration scheme, we consider a contribution g_i^n to Eq. (3), where g_i^n is of the form

$$\begin{aligned} g_i^n &= \sum_j \int_S \vartheta_{ij}(\vec{r})\left\{\frac{1}{\Delta t}\int_0^\infty T^n(t)\psi_j(\vec{r},t)\,\mathrm{d}t\right\}\mathrm{d}S \\ &= \sum_{j,e}\int_{S^e}\vartheta_{ij}(\vec{r})\left\{\frac{1}{\Delta t}\int_0^\infty T^n(t)\psi_j(\vec{r},t)\,\mathrm{d}t\right\}\mathrm{d}S \\ &= \sum_{j,e,q} w_q^e\vartheta_{ij}(\vec{r}_q^e)\left\{\frac{1}{\Delta t}\int_0^\infty T^n(t)\psi_j(\vec{r}_q^e,t)\,\mathrm{d}t\right\}. \end{aligned} \tag{21}$$

Here, the summation index j corresponds to a degree of freedom for the electric field and e is the index for the element which occupies the surface S^e. We use a quadrature scheme with the points $\vec{r}_q^e$ and weights w_q^e for element e, where q is an index for the quadrature points. We partition g_i^n so that it can be expressed in terms of three matrix–vector products and one vector. The partitioning is given by

$$\{g\}^n = [\psi_{+1}]\{E\}^{n+1} + [\psi_0]\{E\}^n + [\psi_{-1}]\{E\}^{n-1} + \{\psi\}^{n-1}, \tag{22}$$

where $[\psi_{+1}]$ is a matrix derived from Eq. (21) based on the appropriate combination of coefficients associated with $\{E\}^{n+1}$ in Eqs. (17)–(20). The matrices $[\psi_0]$ and $[\psi_{-1}]$ are constructed similarly. The vector $\{\psi\}^{n-1}$ represents the rest of Eq. (21) and it is reassembled for each time step, however, given precomputed and stored data which lowers the computation time to some extent.

Summarizing the time discretization of Eq. (3), we time step the system

$$[A_{+1}]\{E\}^{n+1} = [A_0]\{E\}^n - [A_{-1}]\{E\}^{n-1} - (c\Delta t)^2\Big(\{\xi^{zz}\}^{n-1} + \{\zeta^{uu}\}^{n-1} + \{\zeta^{vv}\}^{n-1}\Big), \tag{23}$$

where

$$[A_{+1}] = [M] + \frac{1}{2}(c\Delta t)[B] + (c\Delta t)^2\big(\theta[S] + [\xi_{+1}^{zz}] + [\zeta_{+1}^{uu}] + [\zeta_{+1}^{vv}]\big),$$

$$[A_0] = 2[M] - (c\Delta t)^2\big((1-2\theta)[S] + [\xi_0^{zz}] + [\zeta_0^{uu}] + [\zeta_0^{vv}]\big),$$

$$[A_{-1}] = [M] - \frac{1}{2}(c\Delta t)[B] + (c\Delta t)^2\big(\theta[S] + [\xi_{-1}^{zz}] + [\zeta_{-1}^{uu}] + [\zeta_{-1}^{vv}]\big).$$

Here, the stiffness matrix associated with Eq. (4) is denoted $[S]$, the mass matrix derived from Eq. (6) is $[M]$ and the "loss" matrix stemming from Eq. (7) is $[B]$. It should be noted that Eq. (5) has been partitioned into $[\xi_{+1}^{zz}]\{E\}^{n+1}$, $[\xi_0^{zz}]\{E\}^n$, $[\xi_{-1}^{zz}]\{E\}^{n-1}$ and $\{\xi^{zz}\}^{n-1}$. Similarly, such a partitioning is also applied to Eqs. (8) and (9).

3. Numerical results

We apply the proposed PML formulation to two test cases in order to evaluate its performance and robustness. The tests deal with scattering from infinitely long cylindrical PEC bodies. An incident plane wave $\vec{E}_\mathrm{i}$ is imposed by the application of the boundary condition $\hat{n}\times\vec{E}_\mathrm{s} = -\hat{n}\times\vec{E}_\mathrm{i}$ on the surface Γ_0 of the scatterer, where $\hat{n}$ is the unit vector normal to Γ_0, and we solve for the scattered field $\vec{E}_\mathrm{s}$. The incident plane wave $\vec{E}_\mathrm{i}$ is given by

$$\vec{E}_\mathrm{i}(\vec{r},t) = \vec{E}_0 \exp\left[-\left(\frac{t-\hat{k}_\mathrm{i}\cdot\vec{r}/c - t_0}{d_0}\right)^2\right]\sin\Big[\omega_0(t-\hat{k}_\mathrm{i}\cdot\vec{r}/c - t_0)\Big], \tag{24}$$

which provides a localized pulse in both time and frequency domain. Such an excitation is optimal in the sense that the mean-square time-bandwidth product is the smallest possible [31]. The parameters t_0, d_0 and ω_0 above are chosen so that the frequencies of interest are well excited and the value of $\vec{E}_\mathrm{i}(\vec{r},t)$ is essentially zero on Γ_0 as the computation starts. In Eq. (24), the amplitude with polarization is given by $\vec{E}_0 = E_0(-\hat{x}\sin\phi_\mathrm{i} + \hat{y}\cos\phi_\mathrm{i})$ and the unit wave vector is $\hat{k}_\mathrm{i} = \hat{x}\cos\phi_\mathrm{i} + \hat{y}\sin\phi_\mathrm{i}$, where ϕ_i is the angle of incidence and E_0 controls the magnitude of the incident field. The near-to-far (NTF) field transformation is applied to a closed contour Γ_NTF, which is located within the vacuum region between the scatterer Γ_0 and the PML extending from Γ_PML. The PML is backed by a boundary condition $\hat{n}\times\vec{E}_\mathrm{s} = \vec{0}$ and we use a

quadratic conductivity profile $\sigma(\varrho) = \sigma_{\max}(\varrho/\delta)^2$, where ϱ is the distance from Γ_{PML} and δ is the thickness of the PML.

The RCS is denoted σ and it is computed from [8]

$$\sigma(\phi_{\mathrm{s}}) = \lim_{r\to\infty} 2\pi r \frac{|\vec{E}_{\mathrm{s}}|^2}{|\vec{E}_{\mathrm{i}}|^2} = \frac{k}{4|\vec{E}_{\mathrm{i}}|^2}\left(|L_z + ZN_\phi|^2 + |L_\phi - ZN_z|^2\right) \tag{25}$$

given the fields in frequency domain, which are computed from the time domain fields by the discrete Fourier transform. Here, k is the wavenumber, ϕ_{s} is the azimuthal angle for the scattered wave direction and Z is the wave impedance. The scattering amplitudes $\vec{N}$ and $\vec{L}$ in Eq. (25) are given by

$$\vec{N} = \oint_{\Gamma_{\mathrm{NTF}}} \vec{J}_{\mathrm{s}}(\vec{r}')\mathrm{e}^{+\mathrm{i}k\hat{r}\cdot\vec{r}'}\,\mathrm{d}L', \tag{26}$$

$$\vec{L} = \oint_{\Gamma_{\mathrm{NTF}}} \vec{M}_{\mathrm{s}}(\vec{r}')\mathrm{e}^{+\mathrm{i}k\hat{r}\cdot\vec{r}'}\,\mathrm{d}L'. \tag{27}$$

Here, we have the source point $\vec{r}'$ and the observation point $\vec{r} = r\hat{r}$, where $\hat{r} = \hat{x}\cos\phi_{\mathrm{s}} + \hat{y}\sin\phi_{\mathrm{s}}$. Furthermore, the equivalent surface currents are given by $\vec{J}_{\mathrm{s}} = \hat{n}\times\vec{H}$ and $\vec{M}_{\mathrm{s}} = -\hat{n}\times\vec{E}$, where $\hat{n}$ is the unit normal pointing away from the region enclosed by Γ_{NTF}.

The matrix $[A_{+1}]$ in Eq. (23) is symmetric positive definite and we found it to be well conditioned for all the problems considered so far. We use the conjugate gradient method to solve the system of linear equations, where an incomplete Cholesky factorization of $[A_{+1}]$ is used as a preconditioner. A relative decrease of 10^{-14} in the residual norm was used as a termination condition for the iterative solver and, with a zero fill-in preconditioner, roughly 10 iterations are required per time step.

3.1. Circular cylinder

The proposed PML formulation is validated against analytical results [32] for a PEC circular cylinder. The bistatic RCS was computed for the grid shown in Fig. 1, where the thickness of the PML is doubled so that we have a discretization with 16 cells in the radial direction. For this particular discretization, we have a typical cell size $h = h_0$ and we use $\sigma_{\max} = \sigma_0$, where $\sigma_0\delta = 0.014$ S. This grid is uniformly refined twice to give $h = h_0/2$ and $h_0/4$ with $\sigma_{\max} = 2\sigma_0$ and $4\sigma_0$, respectively. In the following, we use a time step which satisfies $c\Delta t/h = 0.31$ and denote the diameter of the circular cylinder by d. The integration contour Γ_{NTF} is a circle with the radius $0.6d$ and the PML extends from the radius $0.7d$.

The relative error $e = \|\sigma_{\mathrm{n}} - \sigma_{\mathrm{a}}\|/\|\sigma_{\mathrm{a}}\|$ in the bistatic RCS is shown in Fig. 2 as a function of kd. Here, $\|\cdot\| = [\int_0^{2\pi}(\cdot)^2\,\mathrm{d}\phi_{\mathrm{s}}]^{1/2}$ and σ_{n} and σ_{a} is the numerically computed and analytic bistatic RCS. The number of points per wavelength on the coarsest grid ranges from $\lambda/h_0 = 12.5$ at $kd = 8$ to the Nyquist limit $\lambda/h_0 = 2$ at $kd = 52$. We achieve a relative error less than 2% for $\lambda/h > 10$ and this bound on the error is valid for a broad frequency band, where the lowest frequency corresponds to $\lambda/h \simeq 900$.

In Fig. 3, the error is shown as a function of cell size h for three specific frequencies. Here, the symbols (triangles and circles) show computed errors for $h = h_0$, $h_0/2$ and $h_0/4$ while the lines are least square fits to the model $e \propto h^{\alpha}$. We find that the order of convergence α is limited to $1.4 < \alpha < 2.3$ for $8 < kd < 40$. Deviations from the expected order of convergence $\alpha = 2$ are attributed to the low resolution, mainly for $h = h_0$, which most likely is not within the region of asymptotic convergence. Nevertheless, this is a strong indication that the time domain FEM with PML converges toward the analytical solution with an error proportional to h^2.

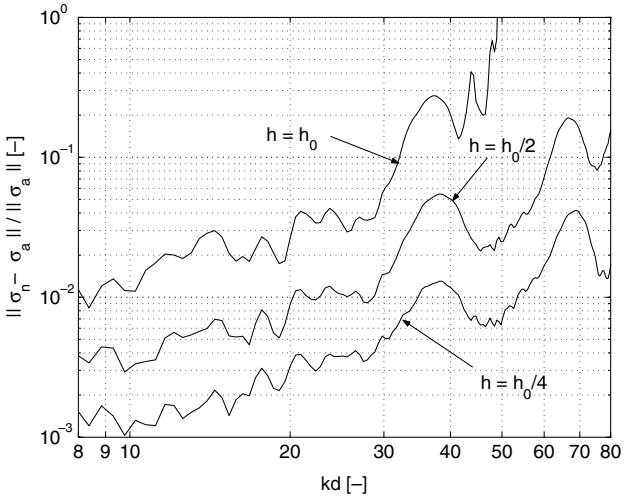

Fig. 2. Relative error in bistatic RCS as a function of kd for three different cell sizes h, where d is the diameter of the circular cylinder and k is the wavenumber. The coarsest grid with $h = h_0$ is refined uniformly to achieve $h = h_0/2$ and $h_0/4$.

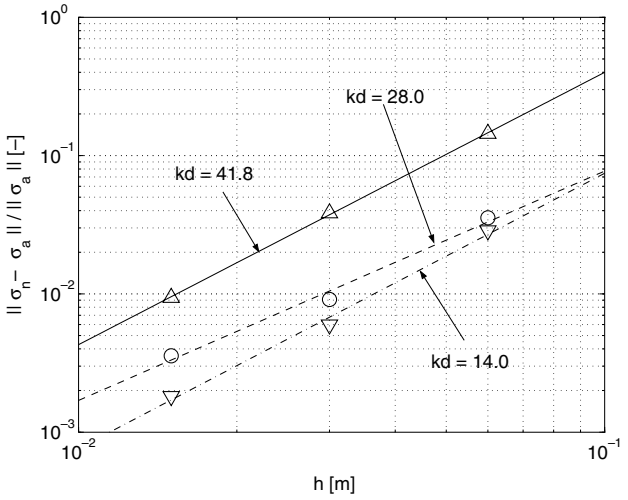

Fig. 3. Relative error in bistatic RCS as a function of the cell size h for three specific frequencies: $kd = 41.8$ – solid line with triangles, $kd = 28.0$ – dashed line with circles and $kd = 14.0$ – dashed-dotted line with triangles. The wavenumber is denoted k and the diameter of the cylinder d.

Fig. 4 shows a sample of the electric field as a function of time, where the sample is taken in the air region between the circular cylinder and the PML. After the transients have decayed ($t/\Delta t > 1500$), the amplitude is reduced six orders of magnitude as compared to the peak value of the scattered wave. We achieve similar results for any point in the air region and this characteristic feature has been repeated for all scatterers studied so far. The post transient field has mainly very high and very low frequency components, which are poorly absorbed by the PML. Extensive numerical tests have not shown any signs of instabilities and these tests include up to 200,000 time steps which satisfy $0.1 < c\Delta t/h < 1.0$.

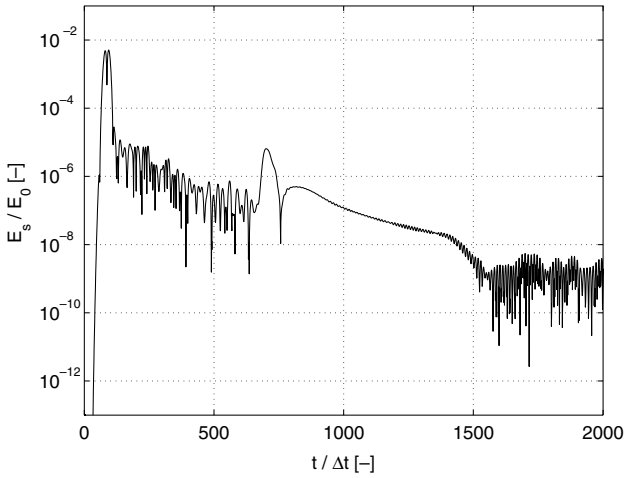

Fig. 4. Sample of the electric field as a function of time. The sample is taken in the air region between the circular cylinder and the PML.

3.2. Ogival cylinder

In the second test case, we compute the monostatic RCS for an ogival PEC cylinder, which has two sharp corners supporting field singularities. Such sharp corners are known to lower the order of convergence [33,34]. The cross section of the ogive occupies the region defined by the union of two circles with the radii $R = (b^2 + a^2)/(2a)$ and the centers along the y-axis at $y = \pm(b^2 - a^2)/(2a)$. Here, we choose the width $2a = 0.2$ m and the length $L = 2b = 1.0$ m. The discretization for the ogival cylinder is shown in Fig. 5, where the grid is truncated by an eight cells thick PML formulated in Cartesian coordinates with $\sigma_{\max}\delta = 0.014$ S. The boundary Γ_{NTF} for the NTF field transformation is indicated by the thick dashed line. Here, we use a time step which satisfies $c\Delta t/h = 0.15$ and the grid has a typical cell size $h = 15$ mm.

We computed the monostatic RCS for the ogive as a function of the azimuth angle measured counter clockwise from the positive x-axis. The monostatic RCS computed by the proposed time domain FEM with PML is shown by circles in Fig. 6 for $L/\lambda = 0.5$ and in Fig. 7 for $L/\lambda = 3.5$. The solid curves show the RCS

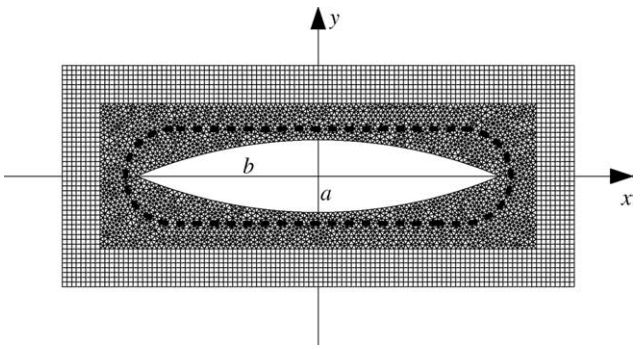

Fig. 5. Discretization of ogive with $a = 0.1$ m and $b = 0.5$ m. The grid is truncated by a PML formulated in Cartesian coordinates and the NTF transformation boundary is indicated by the thick dashed line.

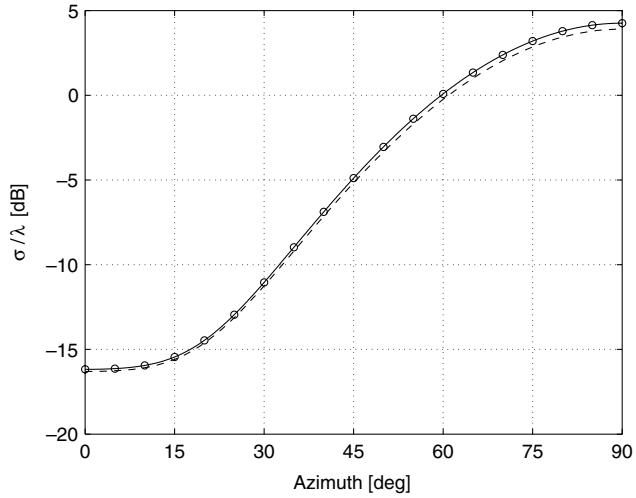

Fig. 6. Monostatic RCS for ogival cylinder with the length 0.5λ: circles – computed RCS, solid curve – spline interpolation of computed RCS, and dashed curve – reference solution.

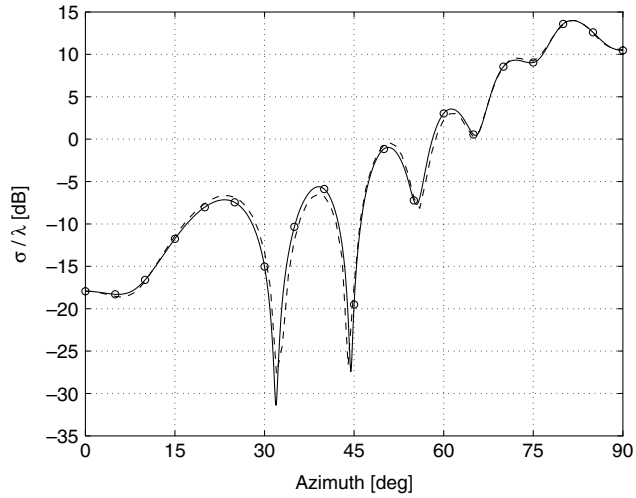

Fig. 7. Monostatic RCS for ogival cylinder with the length 3.5λ: circles – computed RCS, solid curve – spline interpolation of computed RCS, and dashed curve – reference solution.

based on a spline interpolation of the computed complex scattering amplitudes in Eqs. (26) and (27), where we set the slope to be zero at the end points with the azimuthal angle 0° and 90°. The dashed curves show a reference solution computed by the method of moments [35]. We estimate that the reference solution has an error which is less than ± 0.1 dB. For the selected frequencies, we find that the deviation between the RCS computed by the proposed method and the reference solution is less than 1.3 dB except around azimuth angles with deep minima. As previously for the circular cylinder, the computations for the ogive showed no signs of instabilities.

4. Conclusion

We have developed and tested a new formulation for the PML in the context of the time domain FEM. The formulation exploits Galerkin's method in both space and time, where the electric field is expanded spatially in terms of edge elements and temporally as a piecewise linear function. For the free space region, we construct the Newmark time stepping scheme by forming a linear combination of exact and trapezoidal integration for the temporal weak form. This technique is also applied to the convolutions which originate from, in frequency domain, products of the dispersive anisotropic PML materials and the electric field. The convolutions are updated efficiently in time domain by recursive formulas.

The proposed method was tested on scattering of electromagnetic waves from infinitely long PEC cylinders with the cross section shaped as a circle and an ogive. A convergence study of the bistatic RCS for the circular cylinder indicates that the proposed scheme converges toward the analytical result with an error which is proportional to h^2, where h is the typical cell size. We achieve a relative error, in the root-mean-square sense, which is less than 2% when we use more than ten points per wavelength. This bound on the error applies to at least six octaves in frequency. The ogival cylinder has two sharp corners which support field singularities and, for this test case, we computed the monostatic RCS as a function of the azimuth angle for $L/\lambda = 0.5$ and 3.5, where L is the length of the ogive. The computed results were compared to a highly accurate reference solution and we found that, given the selected frequencies, the deviation is less than 1.3 dB except for azimuths where the RCS has deep minima.

Extensive numerical tests have not shown any signs of instabilities and the tests include up to 200,000 time steps Δt which satisfies $0.1 < c\Delta t/h < 1.0$. For the iterative solution of the system of linear equations involved in the time stepping algorithm, the iteration count for one time step is comparable with the corresponding case without the PML material. Therefore, the additional computational cost is associated with the explicit update of the recursive convolutions and this additional work is proportional to the number of cells in the PML. The time integration scheme is directly applicable to three-dimensional problems and it can be adapted to PML formulations for wave phenomena in e.g. acoustics and mechanics. We conclude that the new time integration algorithm works in a robust way and gives high accuracy for a wide frequency band of operation.

Acknowledgements

This work was supported by a grant from AFOSR under contract number F49620-01-1-0228.

References

[1] J.P. Bérenger, A perfectly matched layer for the absorption of electromagnetic waves, J. Comput. Phys. 114 (1994) 185–200, doi:10.1006/jcph.1994.1159.
[2] K.S. Yee, Numerical solution of initial boundary value problems involving Maxwell's equations in isotropic media, IEEE Trans. Antennas Propag. 14 (1966) 302–307.
[3] W.C. Chew, W.H. Weedon, A 3D perfectly matched medium from modified Maxwell's equations with stretched coordinates, Microwave Opt. Technol. Lett. 7 (1994) 599–604.
[4] Z.S. Sacks, D.M. Kingsland, R. Lee, J.F. Lee, A perfectly matched anisotropic absorber for use as an absorbing boundary condition, IEEE Trans. Antennas Propag. 43 (1995) 1460–1463.
[5] S.D. Gedney, An anisotropic perfectly matched layer-absorbing medium for the truncation of FDTD lattices, IEEE Trans. Antennas Propag. 44 (1996) 1630–1639.
[6] C.M. Rappaport, Interpreting and improving the PML absorbing boundary condition using anisotropic lossy mapping of space, IEEE Trans. Magn. 32 (1996) 968–974.
[7] L. Zhao, A.C. Cangellaris, GT-PML: generalized theory of perfectly matched layers and its application to the reflectionless truncation of finite-difference time-domain grids, IEEE Trans. Microwave Theory Technol. 44 (1996) 2555–2563.

[8] A. Taflove, Computational Electrodynamics: The Finite-Difference Time-Domain Method, second ed., Artech House, Norwood, MA, 2000.
[9] W.C. Chew, J.M. Jin, E. Michielssen, Complex coordinate stretching as a generalized absorbing boundary condition, Microwave Opt. Technol. Lett. 15 (1997) 363–369, doi:10.1002/(SICI)1098-2760(19970820)15:6<363::AID-MOP8>3.0.CO;2-C.
[10] F.L. Teixeira, W.C. Chew, PML-FDTD in cylindrical and spherical grids, IEEE Microwave Guided Wave Lett. 7 (1997) 285–287.
[11] F.L. Teixeira, W.C. Chew, Systematic derivation of anisotropic PML absorbing media in cylindrical and spherical coordinates, IEEE Microwave Guided Wave Lett. 7 (1997) 371–373.
[12] J.M. Jin, The Finite Element Method in Electromagnetics, second ed., Wiley, New York, 2002.
[13] J.Y. Wu, D.M. Kingsland, J.F. Lee, R. Lee, A comparison of anisotropic PML to Berenger's PML and its application to the finite-element method for EM scattering, IEEE Trans. Antennas Propag. 45 (1997) 40–50.
[14] M. Kuzuoglu, R. Mittra, Investigation of nonplanar perfectly matched absorbers for finite-element mesh truncation, IEEE Trans. Antennas Propag. 45 (1997) 474–486.
[15] A.D. Greenwood, J.M. Jin, A novel efficient algorithm for scattering from a complex BOR using mixed finite elements and cylindrical PML, IEEE Trans. Antennas Propag. 47 (1999) 620–629.
[16] A.D. Greenwood, J.M. Jin, Finite-element analysis of complex axisymmetric radiating structures, IEEE Trans. Antennas Propag. 47 (1999) 1260–1266.
[17] H.P. Tsai, Y. Wang, T. Itoh, An unconditionally stable extended (USE) finite-element time-domain solution of active nonlinear microwave circuits using perfectly matched layers, IEEE Trans. Microwave Theory Technol. 50 (2002) 2226–2232.
[18] V. Mathis, An anisotropic perfectly matched layer-absorbing medium in finite element time domain method for Maxwell's equations, IEEE Antennas Propag. Soc. Int. Symp. 2 (1997) 680–683.
[19] D. Jiao, J.M. Jin, An effective algorithm for implementing perfectly matched layers in time-domain finite-element simulation of open-region EM problems, IEEE Trans. Antennas Propag. 50 (2002) 1615–1623.
[20] D. Jiao, J.M. Jin, E. Michielssen, D.J. Riley, Time-domain finite-element simulation of three-dimensional scattering and radiation problems using perfectly matched layers, IEEE Trans. Antennas Propag. 51 (2003) 296–305.
[21] P.G. Petropoulos, Analysis of exponential time-differencing for FDTD in lossy dielectrics, IEEE Trans. Antennas Propag. 45 (1997) 1054–1057.
[22] E. Turkel, A. Yefet, Absorbing PML boundary layers for wave-like equations, Appl. Numer. Math. 27 (1998) 533–557, doi:10.1016/S0168-9274(98)00026-9.
[23] E. Bécache, S. Fauqueux, P. Joly, Stability of perfectly matched layers, group velocities and anisotropic waves, J. Comput. Phys. 188 (2003) 399–433, doi:10.1016/S0021-9991(03)00184-0.
[24] F.L. Teixeira, W.C. Chew, On causality and dynamic stability of perfectly matched layers for FDTD simulations, IEEE Trans. Microwave Theory Technol. 47 (1999) 775–785.
[25] J.A. Roden, S.D. Gedney, Convolution PML (CPML): an efficient FDTD implementation of the CFS-PML for arbitrary media, Microwave Opt. Technol. Lett. 27 (2000) 334–339.
[26] N.M. Newmark, A method of computation for structural dynamics, J. Eng. Mech. Div., Proc. Am. Soc. Civil Eng. 85 (1959) 67–94.
[27] J.C. Nédélec, Mixed finite elements in R^3, Numer. Math. 35 (1980) 315–341.
[28] A. Bondeson, G.Y. Fu, Tunable integration scheme for the finite element method, Comput. Phys. Commun. 66 (1991) 167–176, doi:10.1016/0010-4655(91)90065-S.
[29] T. Abboud, J.C. Nédélec, J. Volakis, Stable solution of the retarded potential equations, Applied Computational Electromagnetics Society (ACES) Symposium Digest, 17th Annual Review of Progress, Monterey, CA, 2001, pp. 146–151.
[30] J.F. Lee, R. Lee, A. Cangellaris, Time-domain finite-element methods, IEEE Trans. Antennas Propag. 45 (1997) 430–442.
[31] B. Boashash, Estimating and interpreting the instantaneous frequency of a signal – part I: fundamentals, Proc. IEEE 80 (1992) 520–538.
[32] C.A. Balanis, Advanced Engineering Electromagnetics, Wiley, New York, 1989.
[33] P. Ingelström, L. Lindholm, T. Rylander, Accurate extrapolation to zero cell size by Padé approximation, Int. J. Numer. Model. 16 (2003) 287–298, doi:10.1002/jnm.499.
[34] T. Rylander, A. Bondeson, Application of stable FEM-FDTD hybrid to scattering problems, IEEE Trans. Antennas Propag. 50 (2002) 141–144.
[35] J.M. Jin, V.V. Liepa, Simple moment method program for computing scattering from complex cylindrical obstacles, Proc. Inst. Elec. Eng. H 136 (1989) 321–329.